COMPONENTS' AND MATERIALS' PERFORMANCE FOR ADVANCED SOLAR SUPERCRITICAL CO2 POWERPLANTS

Report on the commissioned particles loop

Deliverable Number 5.1

WP5 Technology validation

Date: 06/10/2023

Deliverable type: Report

Dissemination level: Public

Lead participant: CVR

This project has received funding from the European Union's Horizon 2020 Research and Innovation Action (RIA) under grant agreement No. **958418.**

AUTHORS

Name	Organization
Radomír Filip	**CVR**

DOCUMENT HISTORY

Version	Date	Change
01	06/10/2023	Initial version uploaded

ABOUT THE PROJECT

COMPASsCO_2 is a 4-year HORIZON2020 project started on 1.11.2020. It is led by the German Aerospace Center (DLR), with eleven additional partners from seven European countries.

COMPASsCO_2 aims to integrate CSP particle systems into highly efficient s-CO_2 Brayton power cycles for electricity production. In COMPASsCO2, the key component for such an integration, i.e. the particle/s-CO_2 heat exchanger, will be validated in a relevant environment. To reach this goal, the consortium will produce tailored particle and alloy combinations that meet the extreme operating conditions in terms of temperature, pressure, abrasion and hot oxidation/carburization of the heat exchanger tubes and the particles moving around/across them. The proposed innovative CSP s-CO_2 Brayton cycle plants will be flexible, highly efficient, economic and 100% carbon neutral large-scale electricity producers.

The research focus of COMPASsCO2 is on three main technological improvements: development of new particles, development of new metal alloys and development of the heat exchanger section.

DISCLAIMER

This project has received funding from the European Union's Horizon 2020 Research and Innovation Action (RIA) under grant agreement No. **958418.**

TABLE OF CONTENTS

LIST OF FIGURES

LIST OF ABBREVIATIONS

COMPASsCO2	Components' and Materials' Performance for Advanced Solar Supercritical CO2 Power Plants
CST	Concentrating Solar Thermal
EC	European Commission
EU	European Union
PID	Process and instrumentation diagram
CFD	Computational fluid dynamics
HX	Heat exchanger
sCO2	Supercritical carbon dioxide

1 ABSTRACT

In pursuit of achieving the objectives outlined in WP5, which aims to test the particle heat exchanger under conditions relevant to the project, the implementation of both a hot particle loop and a sCO2 loop is necessary. The hot particle loop must fulfill several critical functions, including heating particles to temperatures as high as 800°C, conveying these heated particles with an appropriate mass flow rate, capturing the particles after passing through the test chamber and subsequently transferring them up to a container upstream of the heater.

To meet these requirements and ensure the safe handling of particles at high temperatures within the loop, several subsystems have been thoughtfully designed, manufactured, and tested to validate the particle loop functionality. The particle loop as a whole, along with each of its individual subsystem are described in detail in their corresponding subsection, filled with comments and insights gathered during numerous experimental campaigns.

2 PARTICLE LOOP DESCRIPTION

Before integrating the sCO2/particle heat exchanger into the particle loop, it was necessary to initially showcase the ability to handle the particles safely and mitigate any potential technological issues. For this reason, a particle loop was designed to test and validate the particles heating and transportation technologies. The proposed particle loop is represented in the PID scheme illustrated in Figure 1, which allows for the identification of each subsystem, their interconnections, and associated instrumentation. The device function as follows:

The majority of the particles are stored in the hopper, extending down to the screw conveyor. When the screw conveyor is active, it starts to carry away the particles from the bottom and the particles from the top start to slide down through the particle heater. There, heat energy is transferred to the particles through an array of electrically heated ceramic tubes. Adjusting the angular velocity of the screw conveyor enables relatively precise control over the mass-flow rate. After leaving the screw conveyor, the particles are mixed with a stream of air, which propels them upwards towards the cyclone separator. Here, the particles are efficiently separated from the air stream and completes the loop.

Since the air transportation operates as an open loop system, employing low-pressure (<10kPa) ambient air, it necessitates treatment before being discharged back to the environment. This precaution is essential as the air carries fine dust particles and retains some heat energy. Consequently, the air is purified in the filtration unit, and some of the residual heat energy is reclaimed through the recuperative heat exchanger.

The particle loop, along with descriptions of its essential components, is presented in Figure 2, while Figure 3 provides a visual representation of its physical construction.

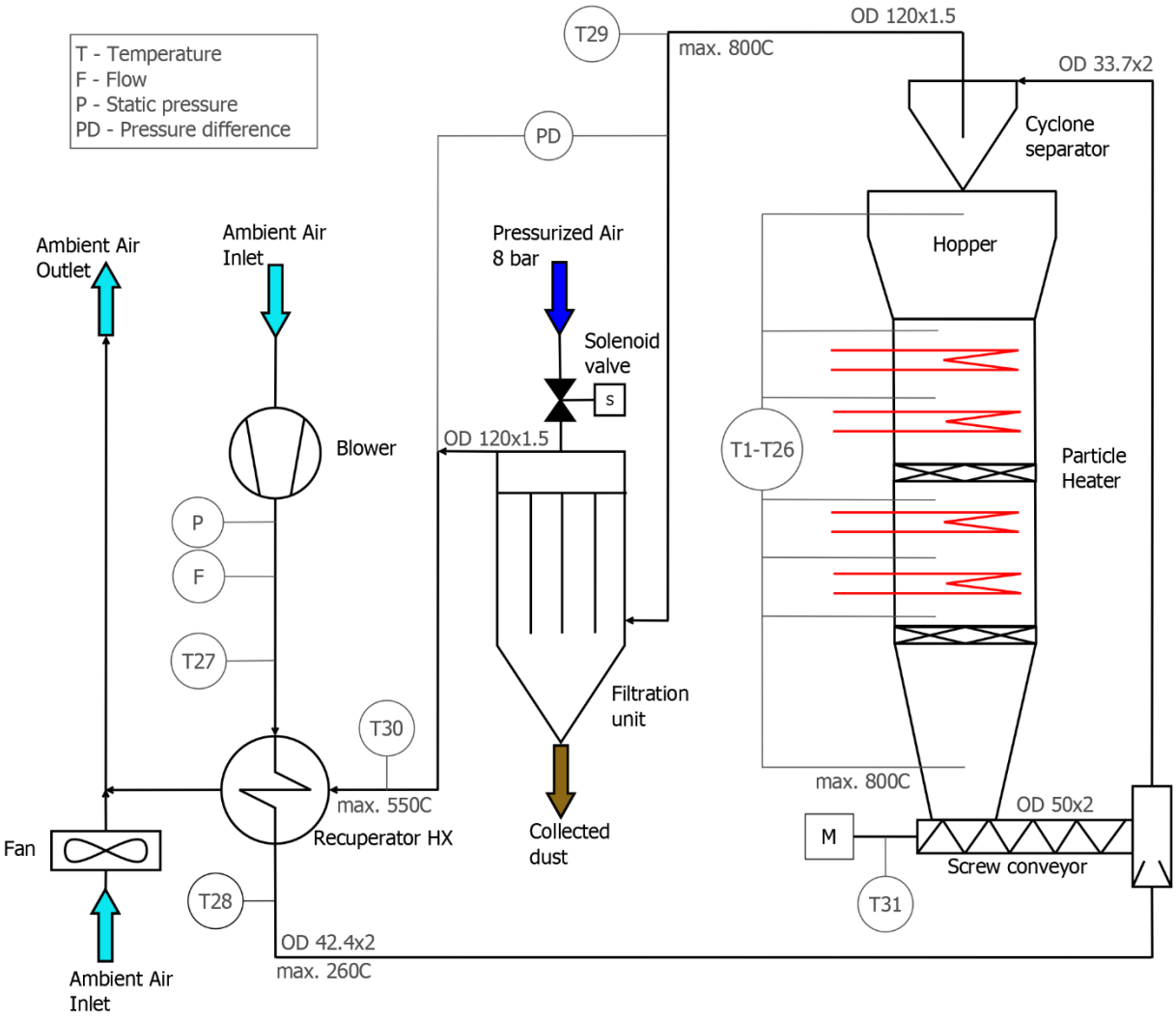

Figure 1: PID scheme of the particle loop.

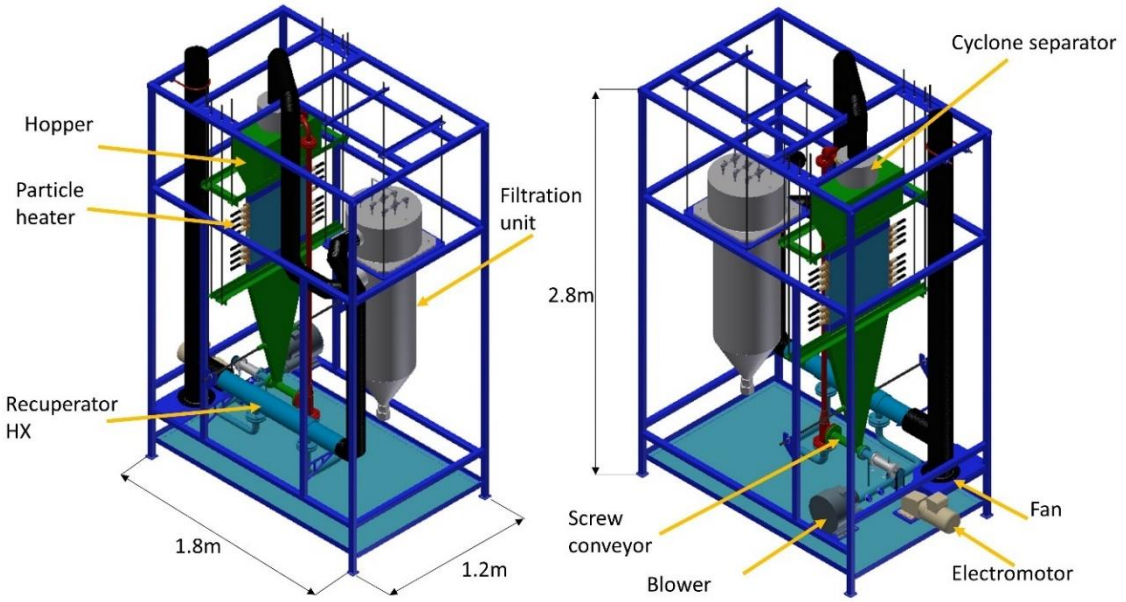

Figure 2: CAD render of the particle loop with marked individual components.

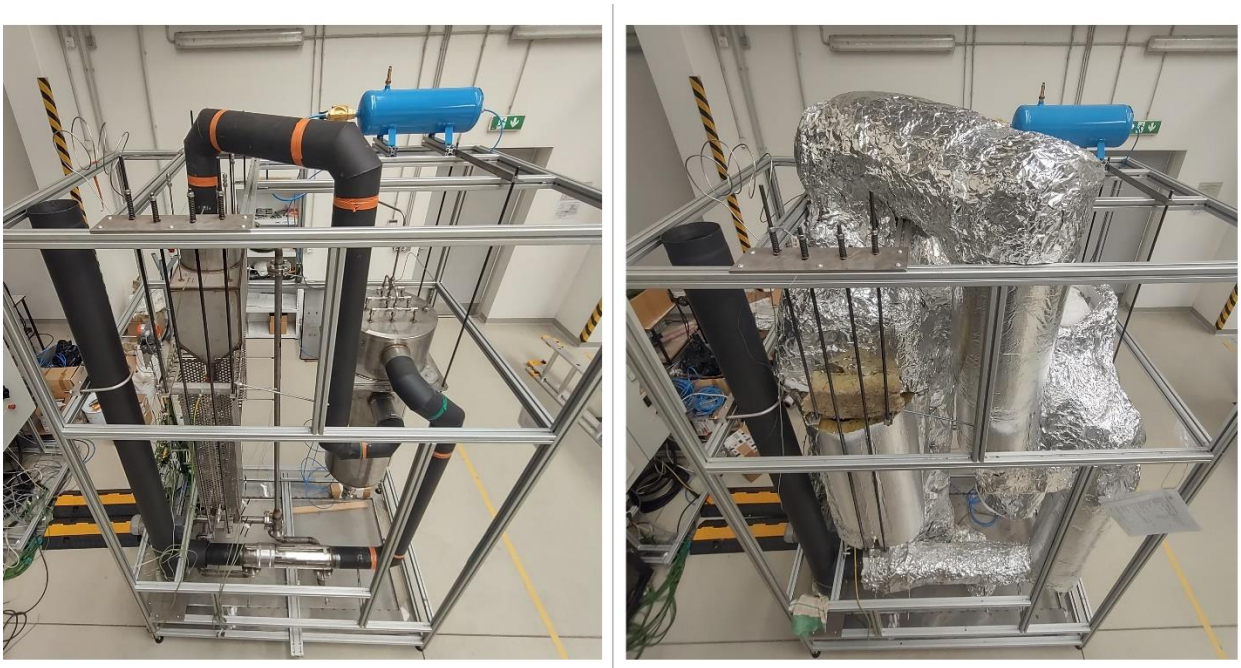

Figure 3: Particle loop, without thermal insulation (on the left), fully thermally insulated (on the right).

2.1 PARTICLE HEATER

This section provides a comprehensive description of the particle heater design. Its representation is shown in Figure 4, along with its outer dimensions and instrumentation ports. The heating process occurs within a single narrow channel, carefully designed and experimentally verified to minimize stagnation zones over the heating tubes, thereby maximizing the convective heat transfer. This achievement results from selecting an appropriate vertical pitch between the heating tubes and utilizing half-tube elements at the sidewalls to ensure homogenous particle flow.

The particle heater comprises eight heating elements divided into two sections. To homogenize the temperature profile, a static mixer is strategically placed between these sections. Figure 5 illustrates a cross-section of the heating zone. Additionally, a second static mixer is positioned in the bottom hopper directly beneath the heater zone, as depicted in Figure 6. The entire heater assembly is suspended from threaded rods anchored in the frame to allow for thermal expansion.

Each ceramic tube can accommodate a heating element with total power input up to 1500 W, allowing for a total heat input of up to 12 kW. Two types of heating elements were tested. Firstly, a heating rod based on silicon carbide, that can theoretically operate at maximum temperatures up to 1600 °C. Secondly, heating elements made of helically coiled resistive wire (Kanthal A1) with a maximum continuous operation temperature of 1400 °C.

The particle heater is equipped with various ports for thermocouples, placed in the second and the last tubes row (shown in Figure 4). These ports are positioned at two distinct zones along the heater tube. The schematics representation of the temperature measurement arrangement is presented in Figure 7. In this setup, two thermocouples are responsible for measuring the

wall temperature, while two others are located upstream and downstream relative to the heated tube. Hence, a total number of 16 thermocouples are used solely for monitoring the particle heater zone.

Beyond these thermocouples, additional temperature measurement points are incorporated into the system. Under the second static mixer in the lower portion of the particle heater, a ceramic tube runs along the channel. It features four holes that can accommodate thermocouples, allowing them to be inserted at varying lengths to monitor the radial temperature distribution. Furthermore, additional four thermocouple ports are located in the bottom hopper (shown in Figure 6). These ports enable direct contact with particles at different heights within the bottom hopper, enhancing the ability to gather more temperature data through the particle outlet.

Figure 8 provides a sneak peek inside the fabricated heater section, showing installed half tubes and a static mixer.

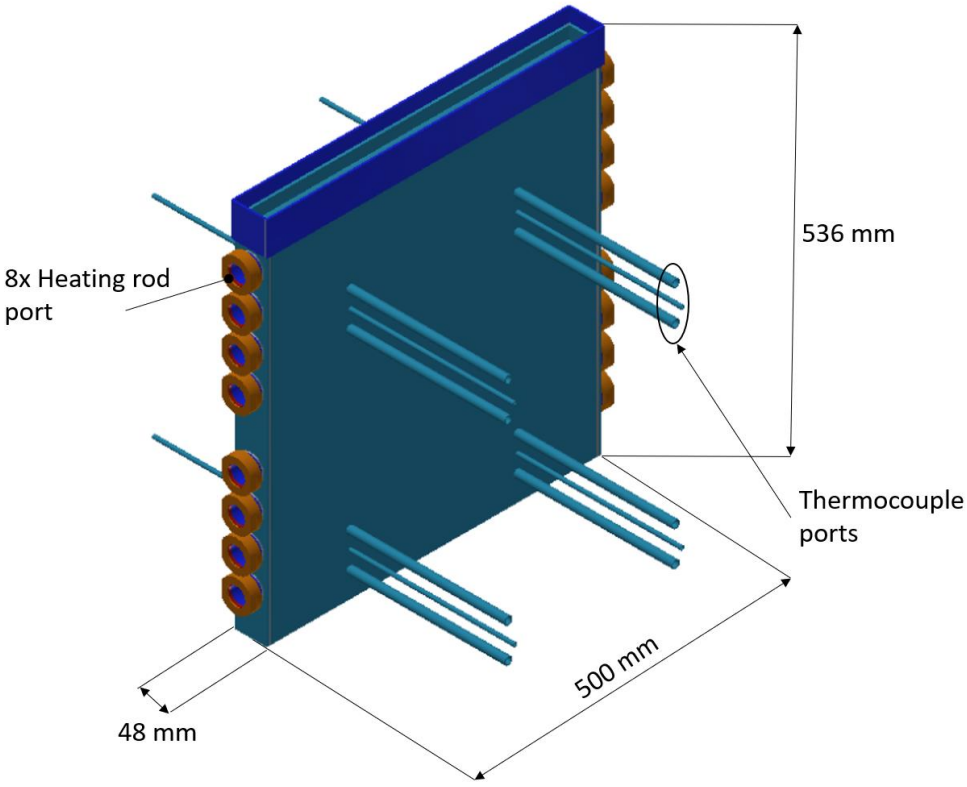

Figure 4: CAD render – Particle heater zone

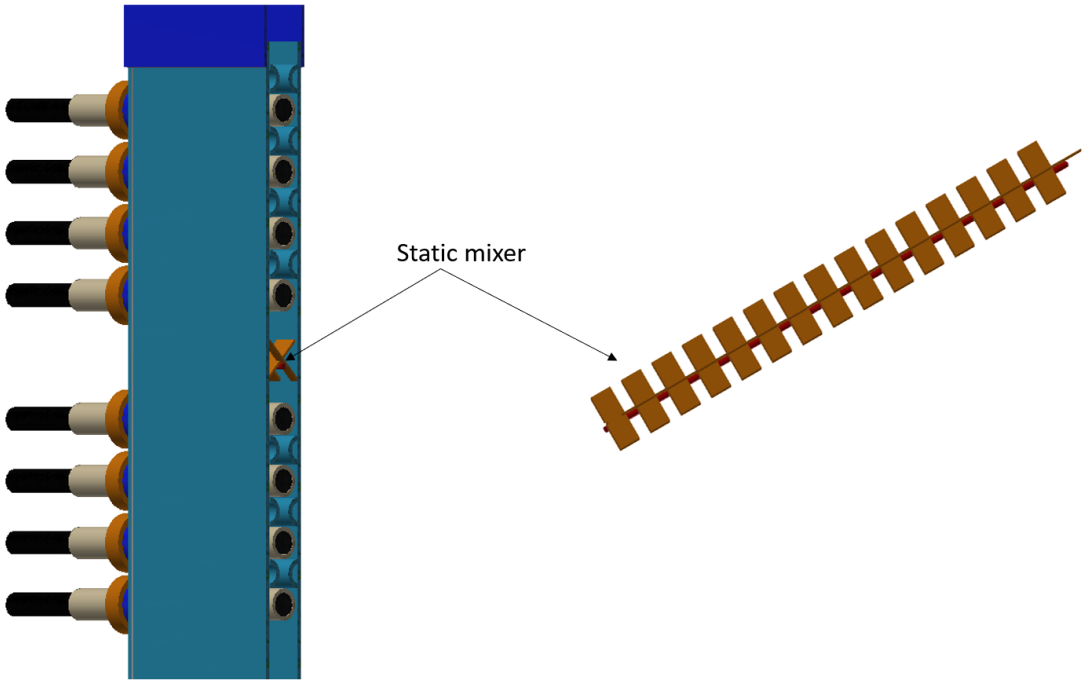

Figure 5: Particle heater – cross-section – static mixer

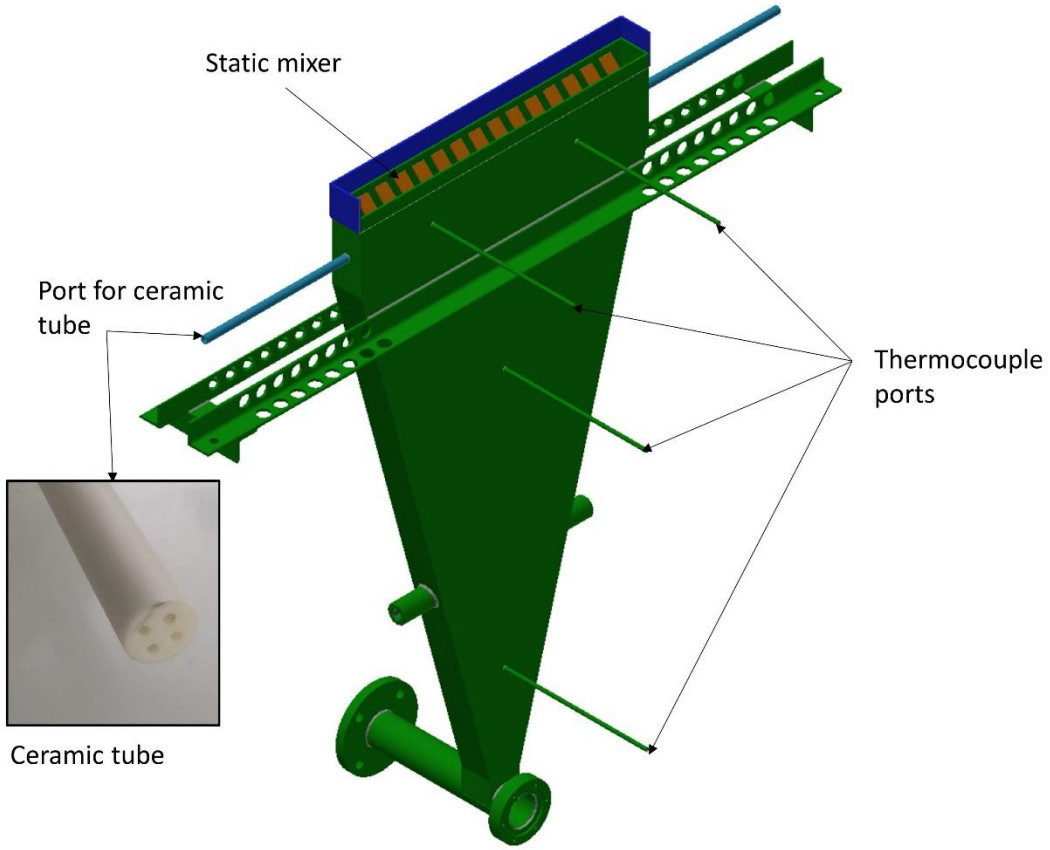

Figure 6: Particle heater - bottom hopper.

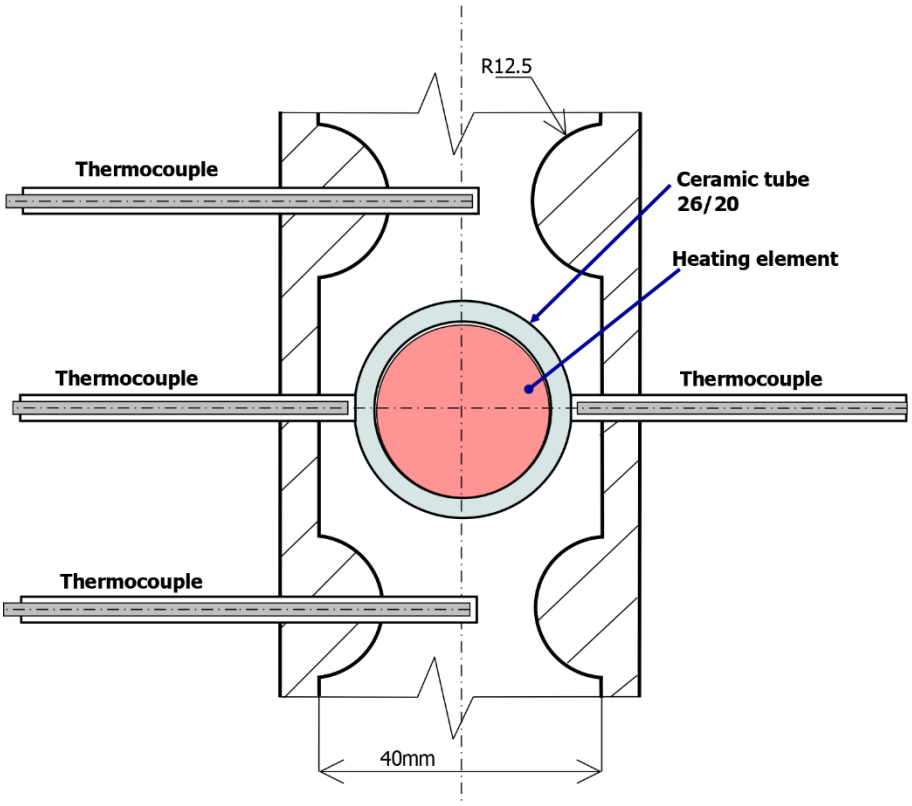

Figure 7: Heater channel schematics with instrumentations.

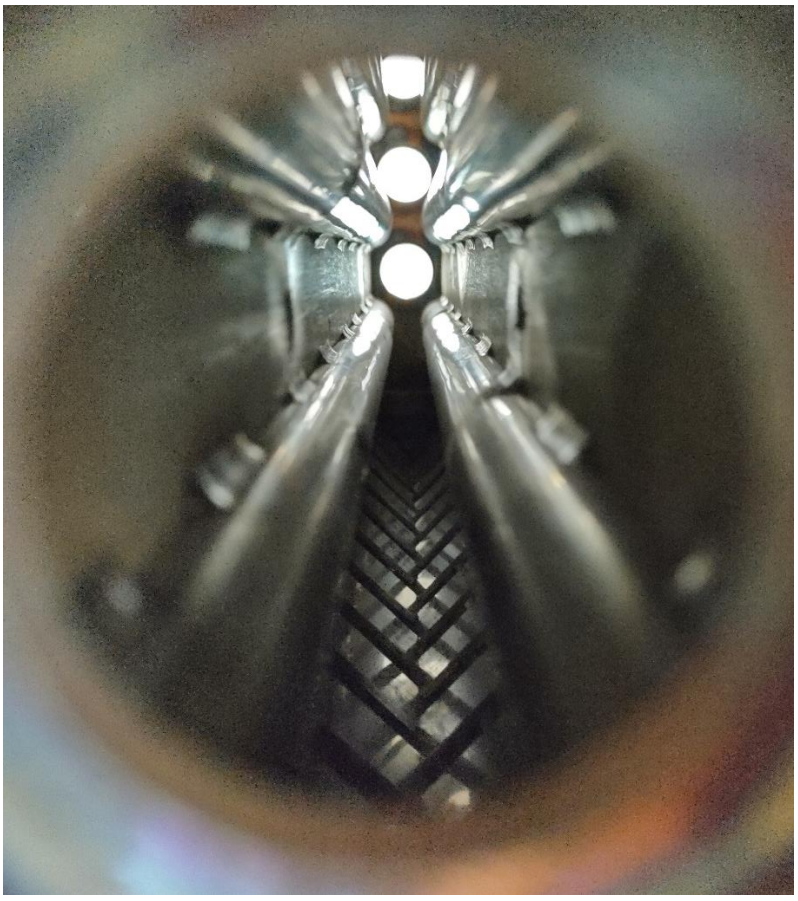

Figure 8: A peek into the interior of the fabricated heater.

2.2 TRANSPORTATION SYSTEM

Particle circulation is facilitated through an open-loop air transportation system, chosen for its relative simplicity and feasibility at the lab scale. This system primarily relies on a screw conveyor, which represents the sole moving component. By adjusting its angular speed, precise control over particle mass flow is achieved. The entire system has been previously operated and validated in experiments using 'cold flow' particles. Consequently, knowledge about expected flow characteristics was gathered, such as particle loading and pressure losses.

However, when operating the system with high-temperature particles (>800 °C), new challenges emerge. Therefore, suitable materials, clearances, and thermal management strategies have been carefully considered to ensure the system's safe and efficient operation.

2.2.1 Screw conveyor

A detailed cross-section view of the transportation system is presented in Figure 9. In this illustration, the conveying screw is attached to a hollow shaft with inner channels, designed to serve as a thermal heat break. Additionally, a small amount of compressed air (40 L/min) is directed through these channels, providing supplementary cooling for the bearings while effectively flushing away potential particle debris. A thermal analysis snapshot is featured in Figure 10, showcasing that, under specified boundary conditions, the bearing temperature should not exceed 60 °C, thereby ensuring reliable continuous operation.

The most critical component of the system is the screw conveyor, which comes into direct contact with the heated particles. It requires to be able operate at high temperatures (up to 800 °C) while enduring the harsh abrasion environment. To address this challenge, the screw was constructed using Nimonic Alloy A80, a material known for its thermal stability up to 815°C and high fatigue strength, even in highly stressed applications. Figure 11 provides a visual representation of the fabricated screw conveyor assembly.

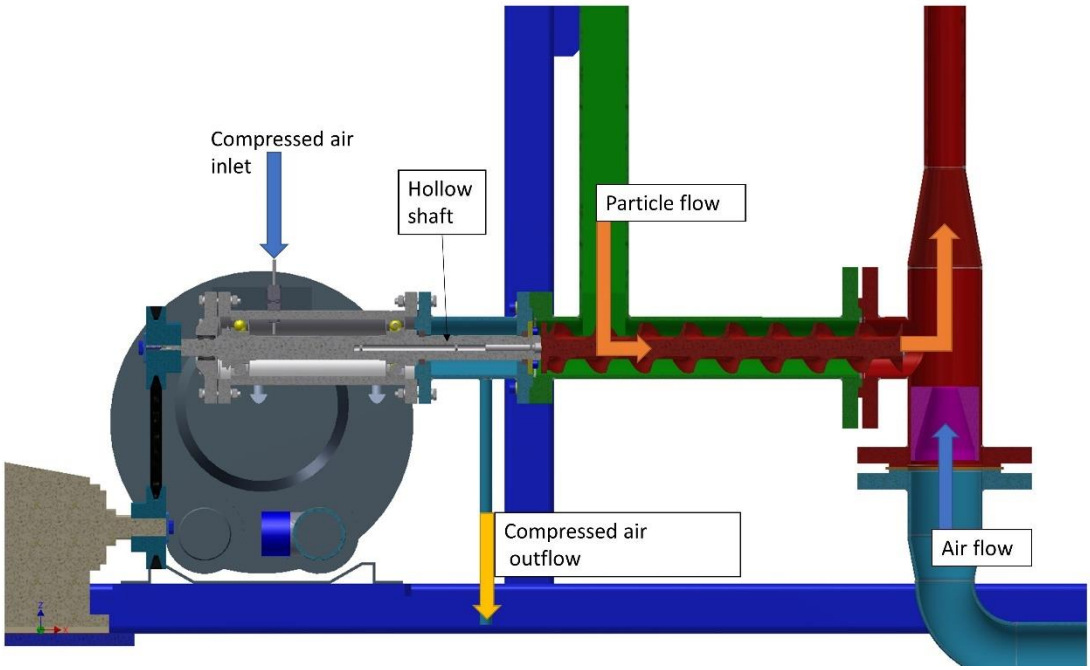

Figure 9: Screw conveyor line – cross-section.

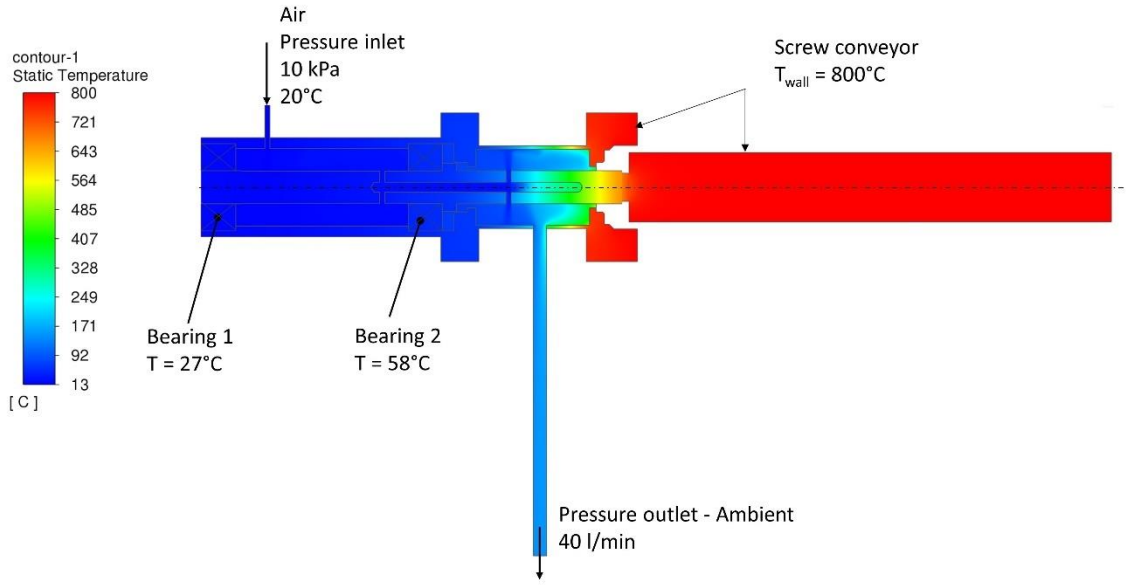

Figure 10: Screw conveyor line – thermal analysis.

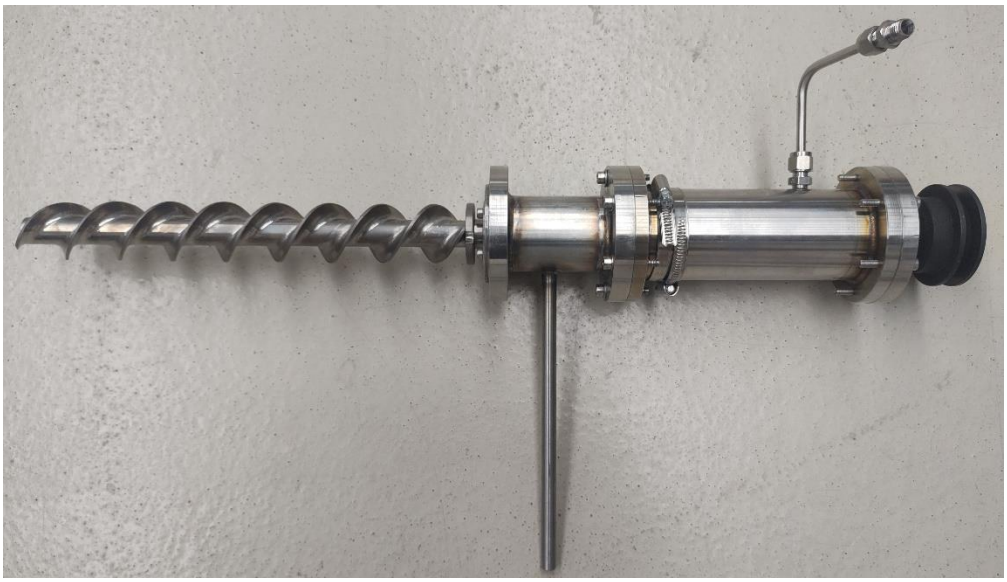

Figure 11: Fabricated screw conveyor assembly.

2.2.2 Cyclone separator

The cyclone separator and the hopper are integrated into a single assembly, with the air/particle mixture entering through a tangential inlet tube (as depicted in Figure 12). As the mixture enters, the air velocity decreases due to the change in flow cross-section, causing it to lose the momentum required to carry the particles. Simultaneously, the particles also decelerate and spiral down into the hopper, where they are stored. However, the outlet air may still carry smaller debris, which is subsequently separated in the filtration unit.

Inside the cyclone separator, an impact plate is positioned to hold material samples for impact test. Its orientation is fixed at a 20° angle relative to the inlet, while the outlet nozzle has been modified to accommodate a larger impact area, as shown in detail in Figure 13. The hopper has a capacity of 100 liter for particle storage and is equipped with four thermocouple ports, enabling temperature monitoring at different locations.

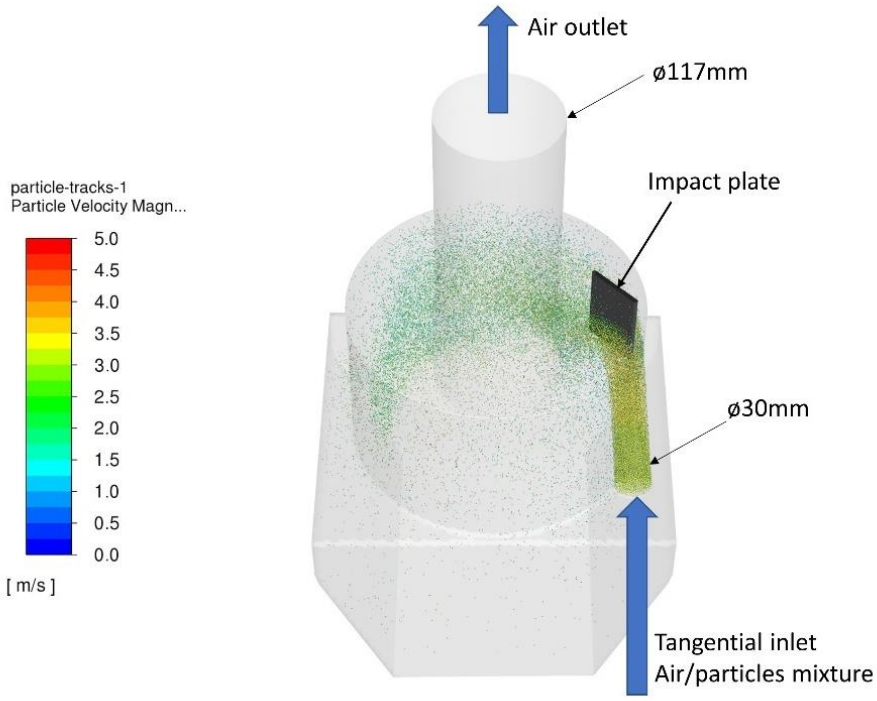

Figure 12: Cyclone separator – particle flow visualization over the impact plate.

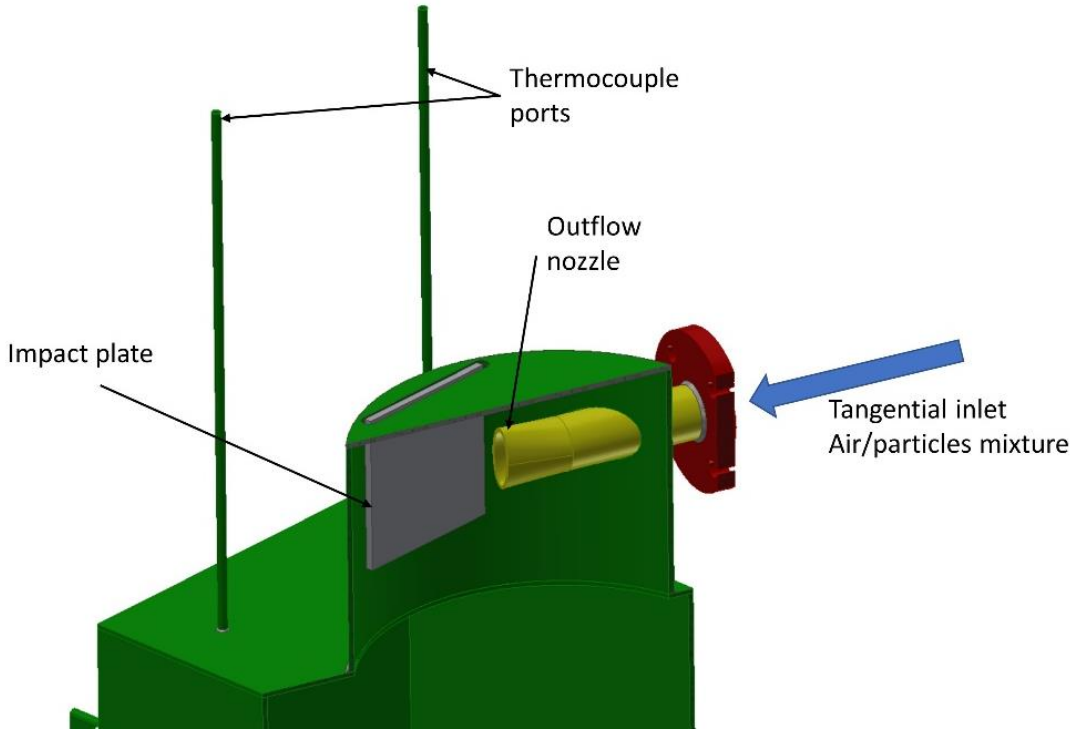

Figure 13: Cyclone separator – a cross-section detail.

2.2.3 Filtration unit

As the air loop operates as an open system, it is imperative to purify the outflowing air before releasing it into the ambient environment. This is essential because the air carries small debris particles as small as 4 μm. To address this issue, a filtration unit was implemented into the

system. The filtration unit features a stainless-steel shell, housing nine ceramic filtration candles capable of operating at temperatures up to 1000 °C, while effectively capturing particles larger than 1 µm, its depiction is shown in Figure 14.

Additionally, the unit is equipped with a compressed air purging system that allows for periodic regeneration of the candle filters. To assess its performance, a CFD analysis of the filtration unit was conducted to evaluate pressure and thermal losses. The results, displayed in Figure 15, show that at estimated boundary conditions (Airflow rate 200 L/min, inlet temperature 700 °C) a pressure loss of 160 Pa and thermal loss of 630 W are achieved, assuming a 100 mm thick thermal insulation.

Notably, the robust design of the filtration unit enables its operation even at higher flow rates, which are anticipated to be double for the final heater test, while still maintaining manageable pressure losses.

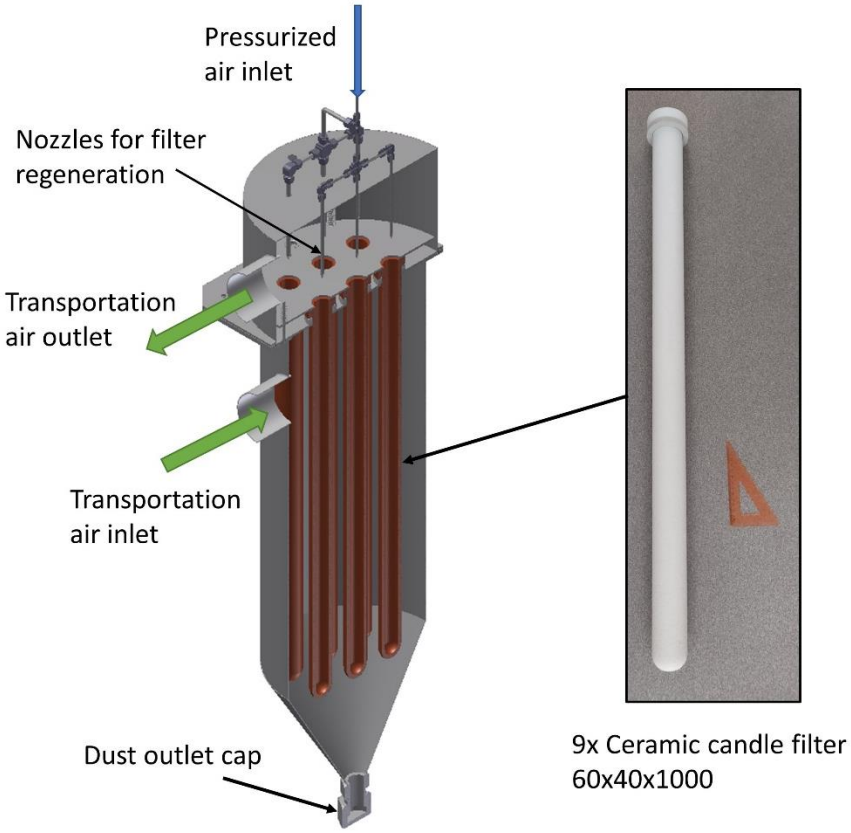

Figure 14: Filtration unit – cross-section

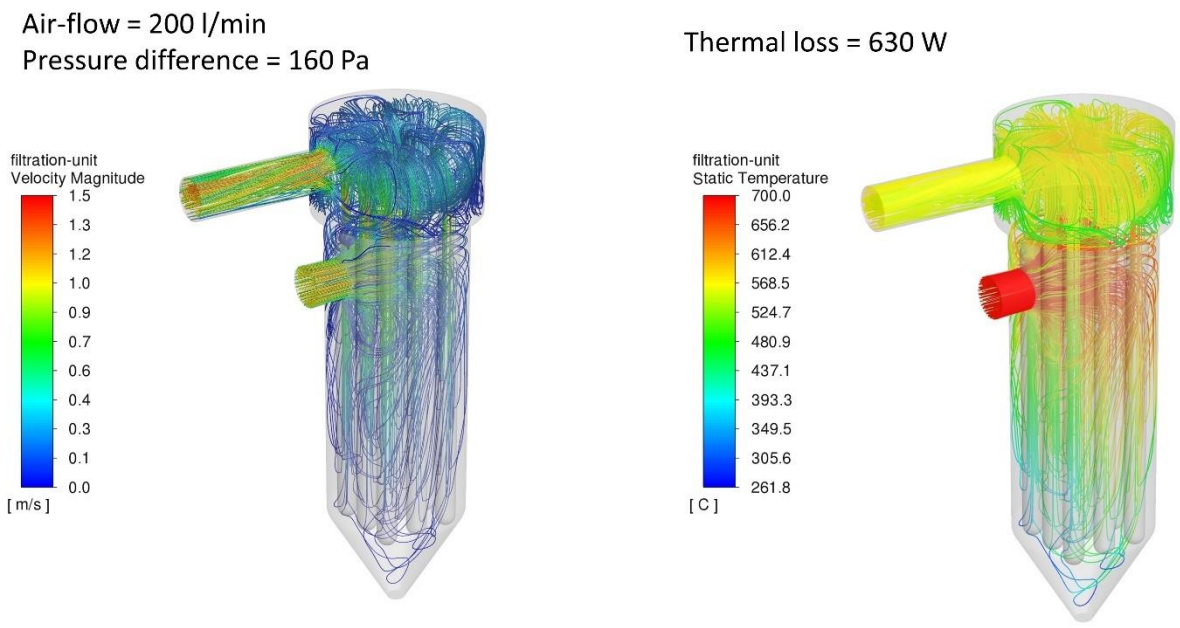

Figure 15: Filtration unit – CFD analysis.

2.2.4 Recuperator heat exchanger

To minimize total heat losses and consequently reduce the energy requirements an air heat recuperator was integrated into the system. Its design involves repurposing a water shell and a tube heat exchanger made of stainless steel, as illustrated in Figure 16. The key modifications include the addition of new welded nozzles on the hot side and the introduction of cut grooves within the shell to accommodate for thermal expansion. These grooves are sealed with a glass fiber thread and a metal sheet sleeve.

A thermal analysis was conducted to validate its performance under the estimated boundary conditions. The results, as presented in Figure 17, indicate its capability to transfer 955 W of thermal energy between the two sides, representing approximately 50% of the available energy. While higher efficiencies can be achieved with different types of heat exchangers that offer increased surface area, it's important to consider the overall recoverable energy, as pursuing such alternatives may not be economically feasible.

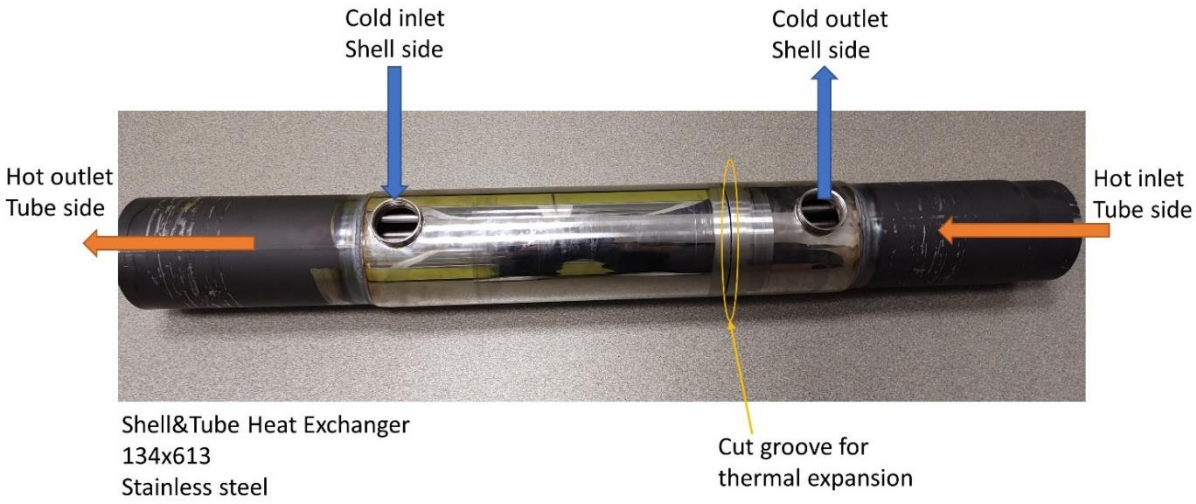

Figure 16: Recuperator HX – physical representation.

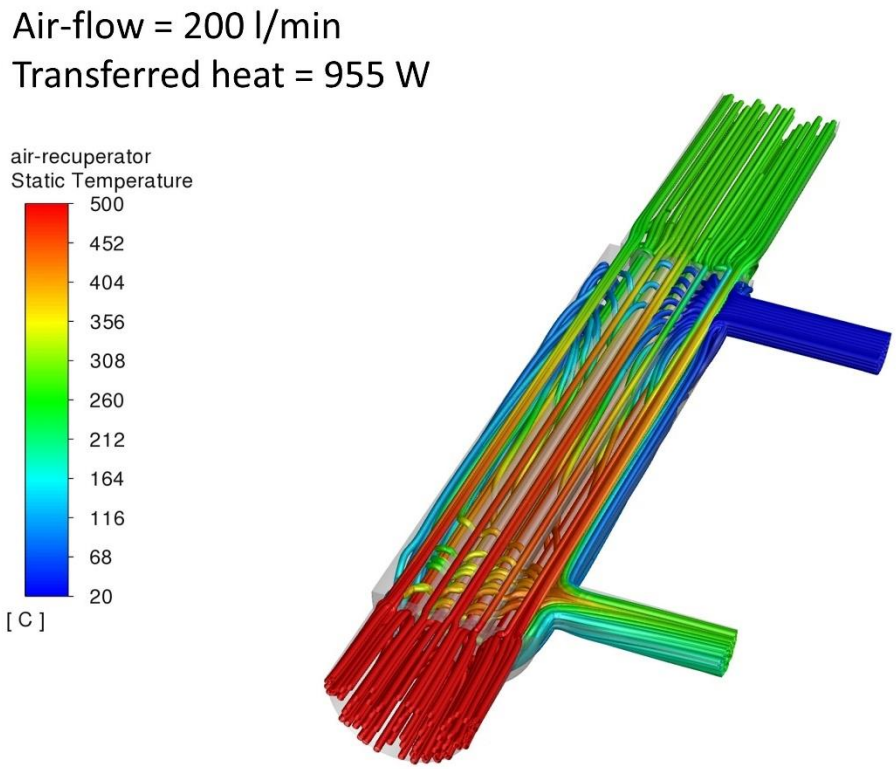

Figure 17: Recuperator HX – Estimated temperature field.

3 COMMISSIONING AND EXPERIMENTS

Finally, several experimental campaigns were performed. These campaigns provided valuable data to assess the particle heater loop performance and the individual component lifetime.

3.1 PARTICLES MASS-FLOW RATE

Precise control of the particle mass-flow is of utmost importance. Therefore, an experimental validation was conducted. For this validation, the particle transportation track was interrupted at the inlet to the cyclone separator and the flow was diverted into a measuring unit. The unit comprises a cyclone separator connected to a small vessel resting on a weigh scale. The measurement schematic is depicted in Figure 18. The flow validation was performed using cold Ferox particles (delivered by Saint-Gobain in the framework of WP2), with a constant air flow while varying the screw conveyor's angular velocity. The mass gain over time was recorded. The resulting particle mass-flow versus the screw revolution speed characteristics is plotted in Figure 19. The measured values fall within a linear trend within the specified range of screw revolution speed, with an error range of ±10%.

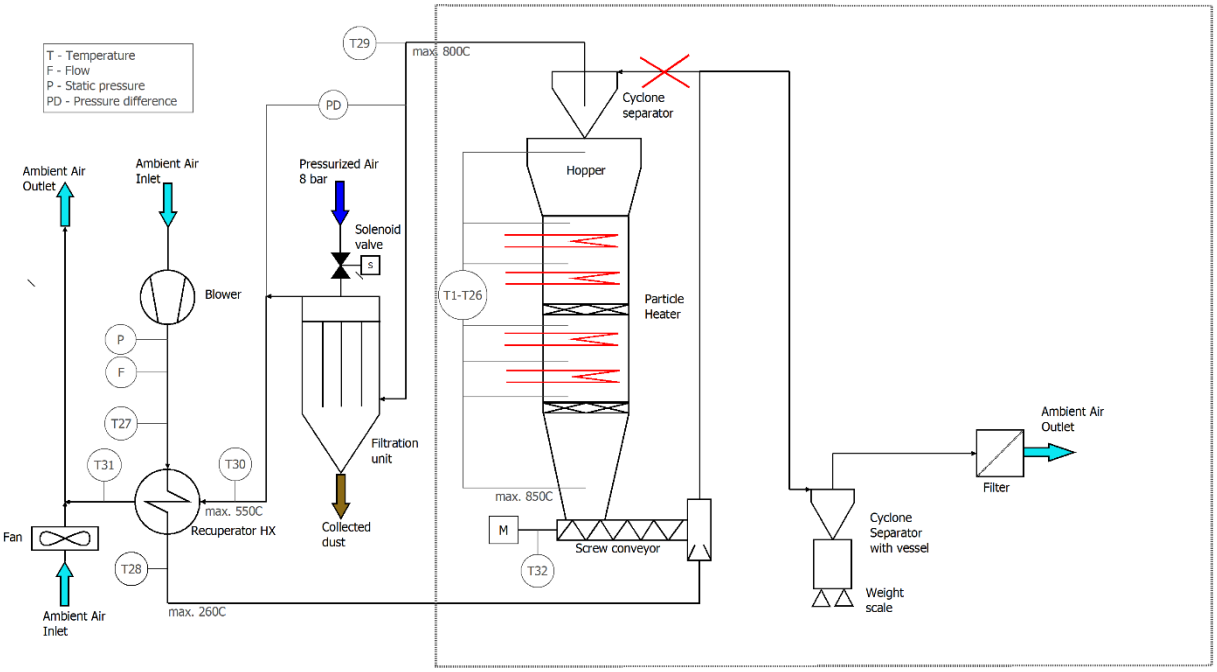

Figure 18: Particle mass-flow measurement schematics.

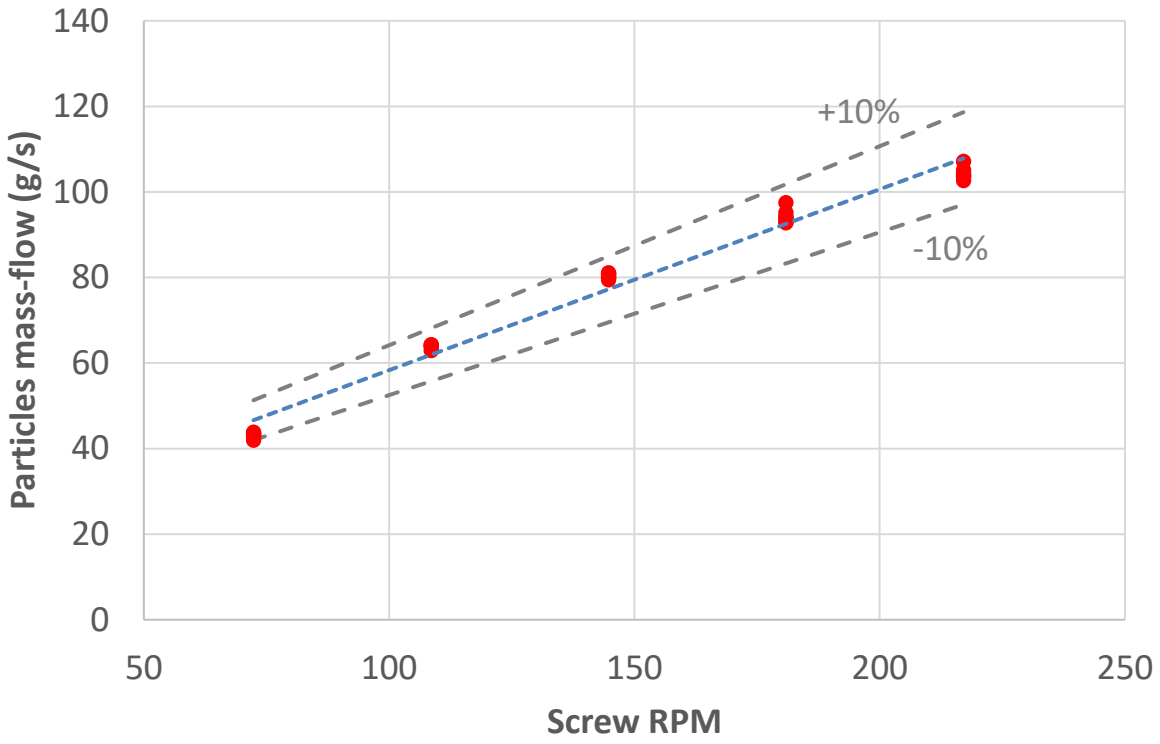

Figure 19: Particle mass-flow characteristics as a function of screw RPM.

3.2 PARTICLES HEATING

Several continuous particle heating campaigns were conducted, during which particles were heated up to 800°C. For a better understanding of the measurement setup, a thermocouple placement map is provided in Figure 20. In Figure 21 and Figure 22, the temperature profiles from a specific measurement experiment corresponding to a particular zone are presented. These profiles reveal several distinct phases that were tested. These are heating, free cooling, forced cooling and holding constant temperature.

The forced cooling phase occurs when the heating is turned off, and the particles are circulated and cooled by the air used for particle transportation. Based on the temperature records, the temperature distribution appears to be relatively symmetric during the first heating stage. However, towards the end of the second heating stage, there is visible temperature asymmetry, with regional overheating compared to the temperatures measured in the middle of the heating zone. This overheating at the sides can be interpreted as local stagnation zones of the particles. This interpretation was later confirmed when the heating elements were replaced, as the last heating element exhibited significant discoloration due to the higher temperature on the left side (shown in Figure 23).

To address the issue with the particle stagnation towards the exit of the heating section, a flow restrainer was installed beneath the heater and thermocouple T18 was moved to the middle of the zone, as illustrated in Figure 24. Initially, a reference measurement was conducted without the restrainer, reaching a steady state with an outlet temperature of 650°C. This was

then repeated with the flow restrainer in place, and the results are presented in Figure 25 and Figure 26.

There is a noticeable change in the particle temperature profile within the first heating stage. In the second stage, the local difference increases up to 40°C, indicating that the flow field improved, resulting in a more effective heat transfer. The most significant improvement occurs in the zone under the heater, where the temperature profile is even on the sides, with only a slight increase in the middle (T18) due to stagnation caused by the close proximity to the flow restrainer. Nevertheless, these differences are much smaller compared to the case without the restrainer, as shown in Figure 26. It is worth noting that the mass-weighted outlet temperature didn't change, since in case without the flow restrainer, the majority of particle flow concentrated in the middle of the zone, leading to stagnant particles and overheating on the sides. However, when the flow restrainer was introduced, it forced particles to flow along the sides. This also influenced the upstream particles, resulting in an improved overall temperature distribution.

On the other hand, the flow restrainer did cause some stagnation in the middle zone, leading to a slight temperature increase in that region. Nevertheless, the maximum temperature difference was smaller when compared to the case without the flow restrainer.

Overall, this solution appears to have a positive impact on temperature distribution and will be implemented in a final test with a particle/sCO2 heat exchanger.

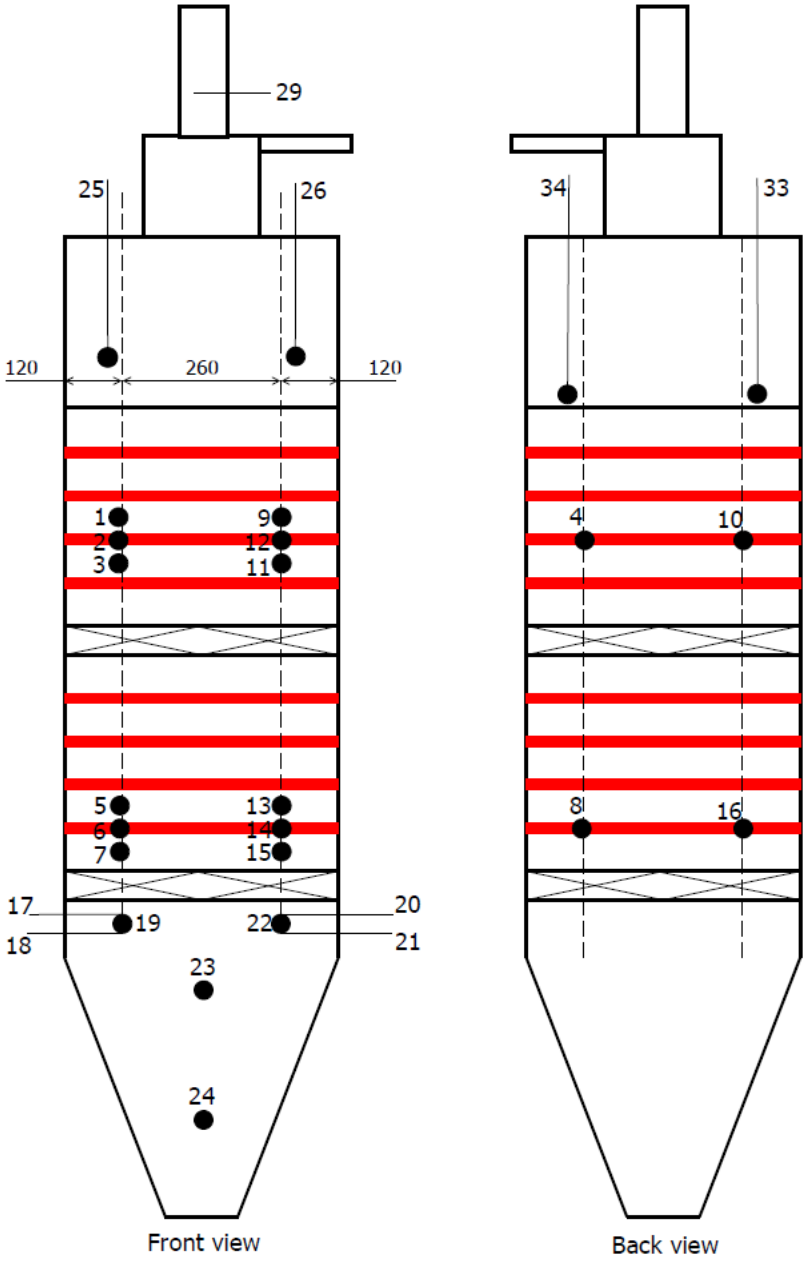

Figure 20: Thermocouple placement map (dots indicate thermocouple positions).

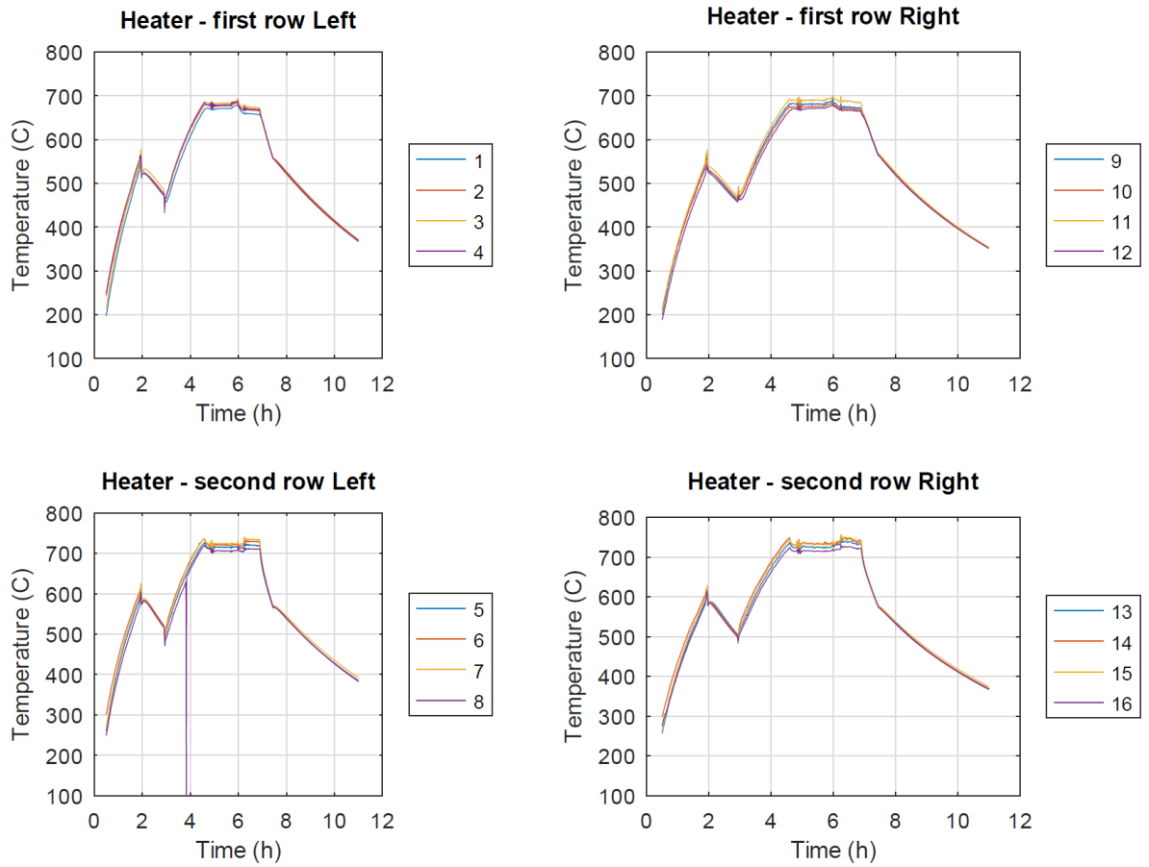

Figure 21: Temperature records within the heater.

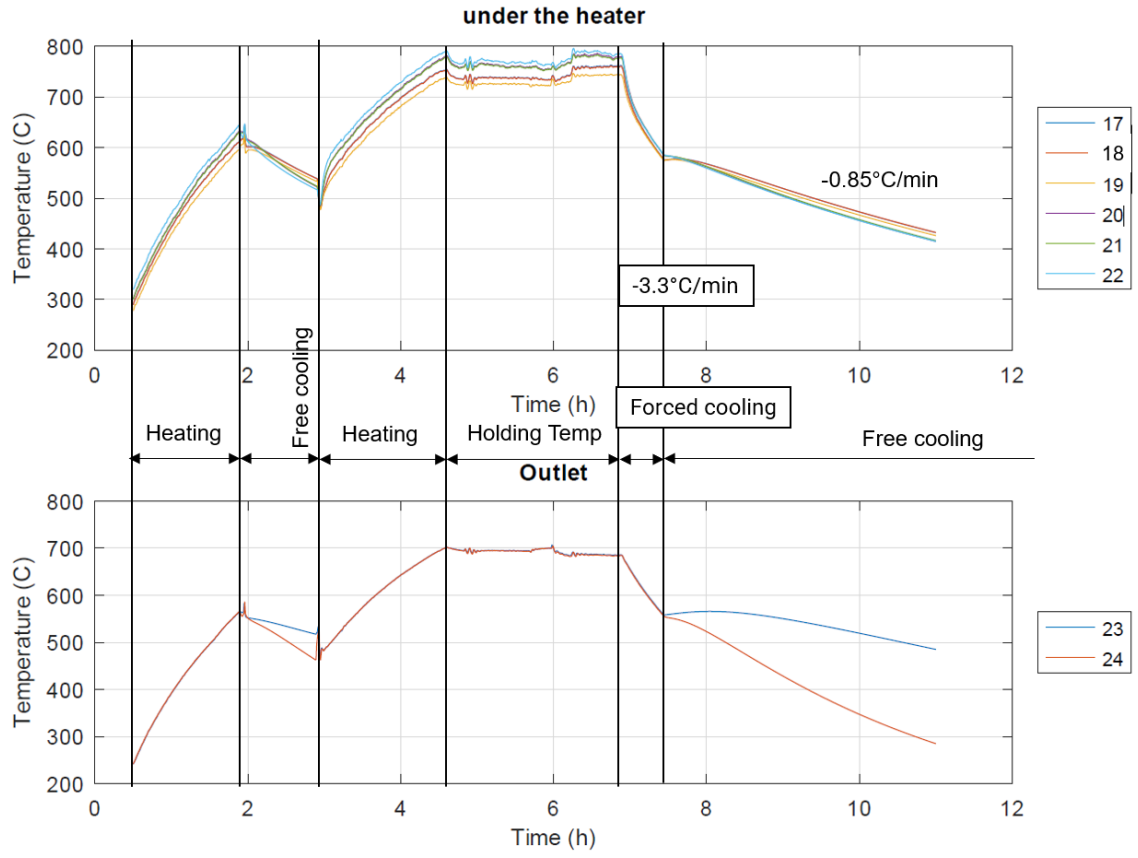

Figure 22: Temperature record under the heater.

Figure 23: SiC heating elements from the last heating stage.

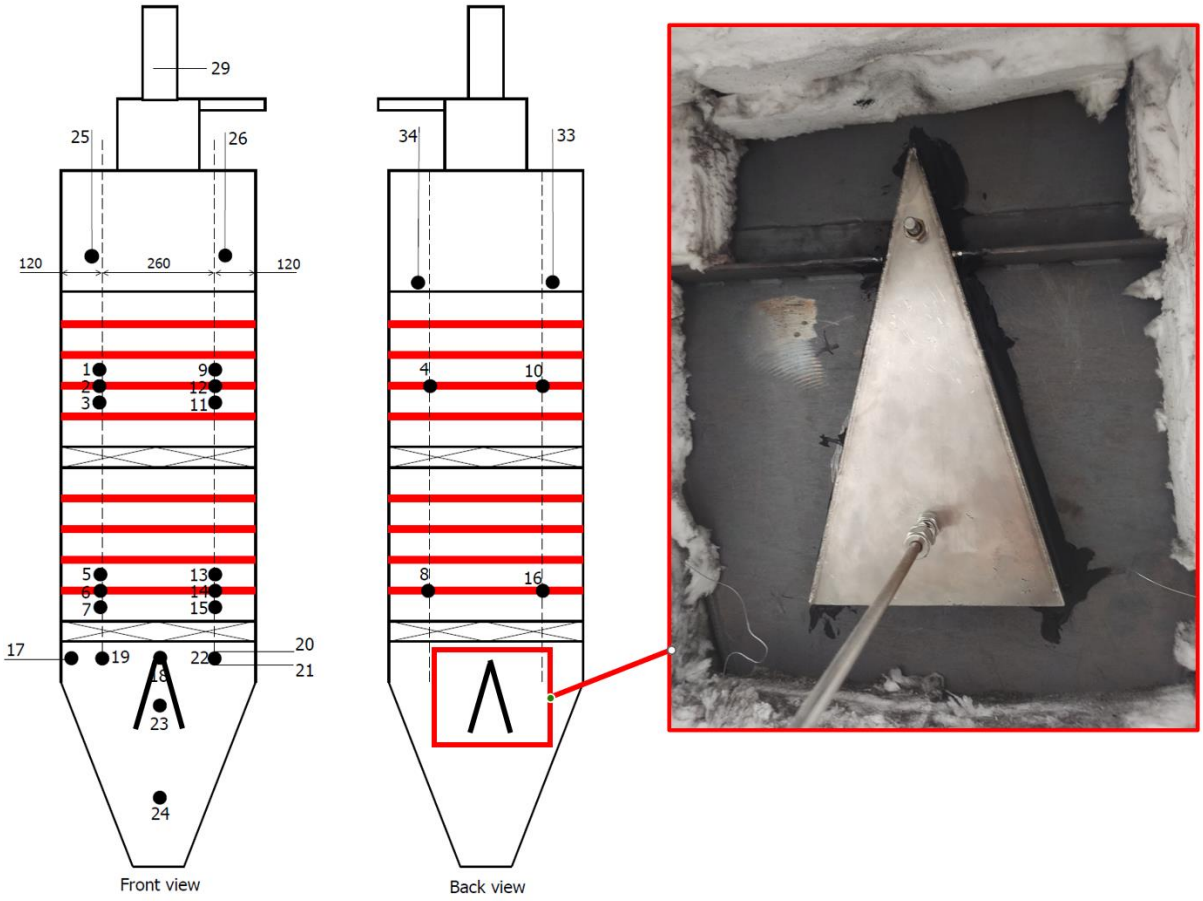

Figure 24: Particle heater - flow restrainer modification with slightly rearranged thermocouples.

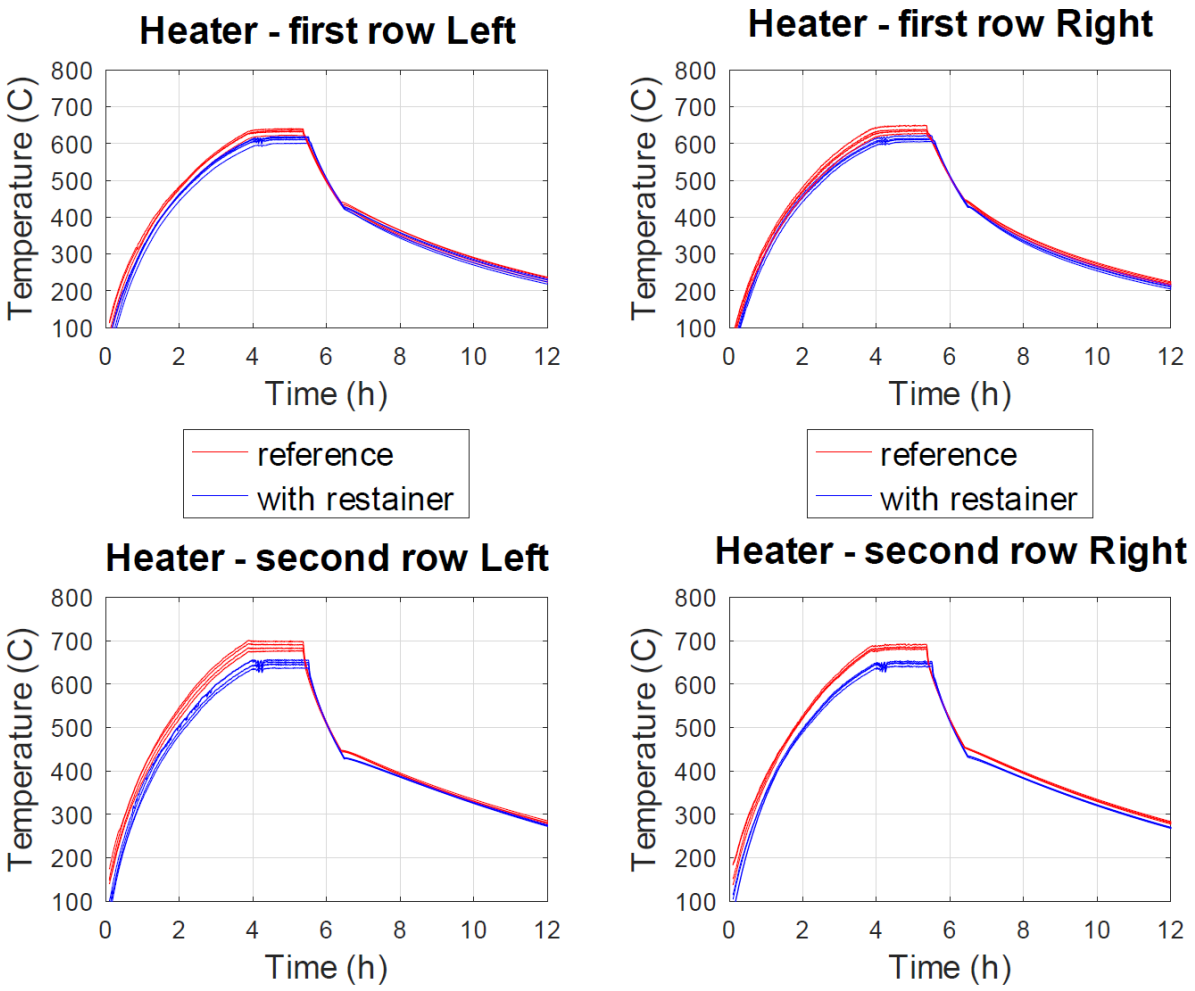

Figure 25: Temperature measurement comparison with and without the flow restrainer – heater zone.

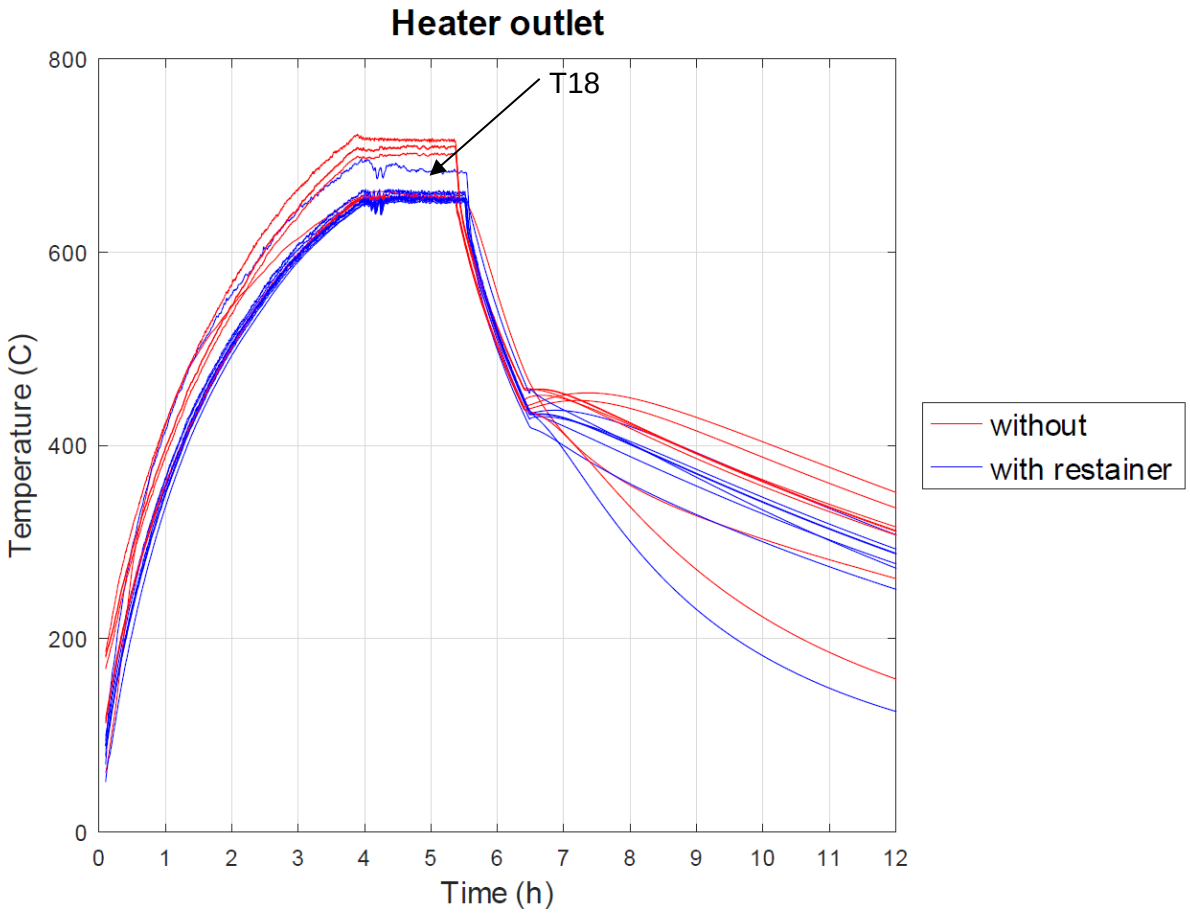

Figure 26: Temperature measurement comparison with and without the flow restrainer – under heater zone.

3.3 HEAT PERFORMANCE EVALUATION

Firstly, the heat losses are estimated from the forced cooling regime, where the temperature change is highly linear, resulting in a constant temperature change over time. The heat loss can be expressed as:

$$Q_{loss} = (m_p\, c_p + m_{steel}\, c_{p_{steel}}) \frac{\Delta T}{t} \qquad (1)$$

In this equation, m_p represents the mass of the particles within the loop, which was measured prior to the experiment and found to be 70,47 kg. C_p denotes the heat capacity of the particles, for which a constant value of 1050 J/kg/K as measured by project partners was considered. Furthermore, the mass and heat capacity of the heater construction material must be taken into account. The corresponding mass, obtained from the CAD model, is 110 kg, and the heat capacity for the stainless steel is 500 J/kg/K. The temperature change over time was determined as an average value of all measured temperatures within the particle zone, resulting in a value of 3.28°C/min.

The resulting overall heat loss is approximately 7 kW, which roughly corresponds to the measured heat input during steady-state operation (holding temperature regime). Furthermore, the heat loss attributed to air transportation itself was estimated within the same case. Taking

into account the temperature difference between the air temperatures T29 and T28 (see Figure 27), air heat capacity and measured air mass-flow, a value of 3.2 kW was determined, which corresponds to 45% of the overall losses.

The impact of the heat recuperator was assessed using the same approach, considering the temperature difference between T28 and T27, resulted in a heat recuperation of 420W, which corresponds to approximately 6% of the overall losses.

To estimate the performance of the heat recuperator, one must consider the available energy before the hot inlet. By measuring the temperature T30, which reached approximately 260°C, it was determined that the heat exchanger efficiency is around 45%, This figure aligns closely with the CFD estimation. The lower-than-expected heat recovery can be attributed to potential small leaks of hot air within the line leading to the filtration unit and increased heat loss due to the extensive surface area of the insulated line and the filtration unit itself. This is supported by the fact that the airflow heat capacity, defined as the product of the mass-flow and heat capacity, is only about 6 W/°C. In simple terms, when a small amount of energy is transferred, it results in a larger temperature drop for a relatively equivalent energy loss

It should be noted that the heat loss due to the transportation will remain for the same particle loading nearly unchanged for a scaled up system. The remaining heat losses are rather high, mainly due to the high volume/surface ratio and despite the amount of thermal insulation the heat loss coefficient can be considered 2-3 W/m^2/K.

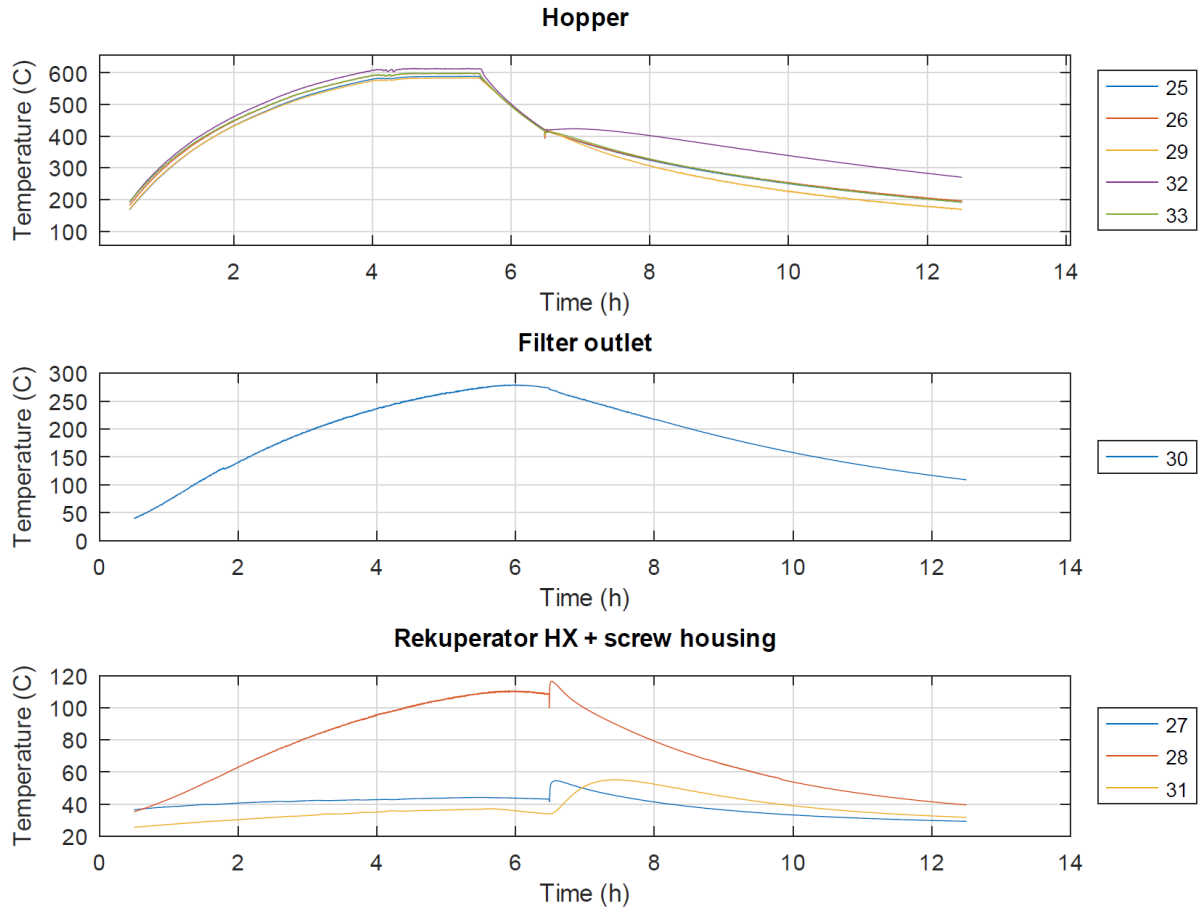

Figure 27: Measured temperatures within the respected zone.

3.4 CRITICAL COMPONENTS ASSESSMENT

The screw conveyor is regarded as a critical component since it is the only moving part that comes into direct contact with particles at elevated temperatures. After 40h of operation, during which temperatures reached up to 700°C, the screw conveyor was removed and inspected. Surprisingly, there were no noticeable structural changes due to the abrasion in the screw geometry. The only visible alteration was the discoloration attributed to the formation of an oxide layer, as shown in Figure 28. This oxide layer provides an additional protection, since the operation temperature falls withing the range typical for the annealing of nickel alloys, which leads to the hardening of the material.

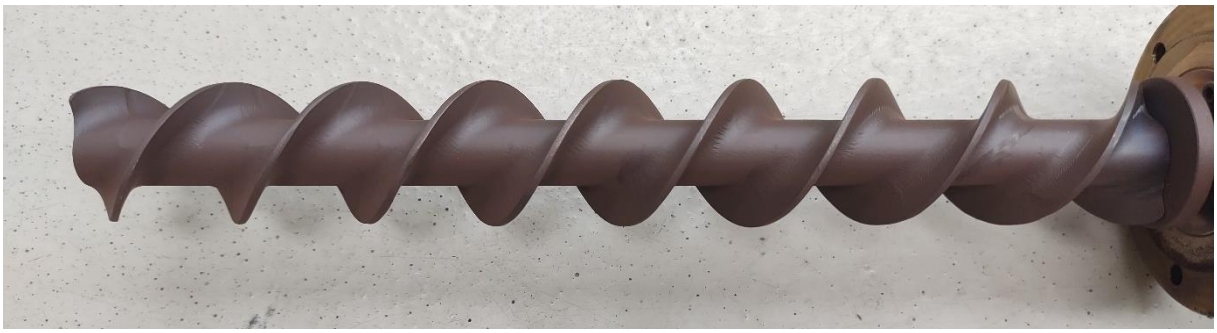

Figure 28: Screw conveyor after 40h of operation.

Another critical component is the knee bend, where the particles change direction from vertical to horizontal before reaching the cyclone separator, where the knee is undergoing severe erosion. This effect becomes more pronounced at elevated temperatures due to the softening of the material and the increased particle velocity within the conveying line. As the air heats up from contact with the particles, it rapidly expands, increasing the velocity of the particles up to 15 m/s, as shown in the results of the analysis (illustrated in Figure 30). This high velocity can have a devastating effect on the structural integrity of the knee bend, as shown in Figure 29.

To extend its life time, the wall within the bend was reinforced with additional welded material. However, it is crucial to periodically inspect and check this component during the long-term operation to ensure its integrity.

The last assessed component are the particles themselves. In the recent tests using the new FerOX particles, it is important to consider the amount of dust generated primarily during the process of air transportation. The dust that accumulated within the filtration unit was collected and measured. Based on the dust mass measurements and the total experimental runtime, it was estimated that within 24-hour period, approximately 100g of particles will be lost due to the air transportation, while they undergo roughly 70 cycles.

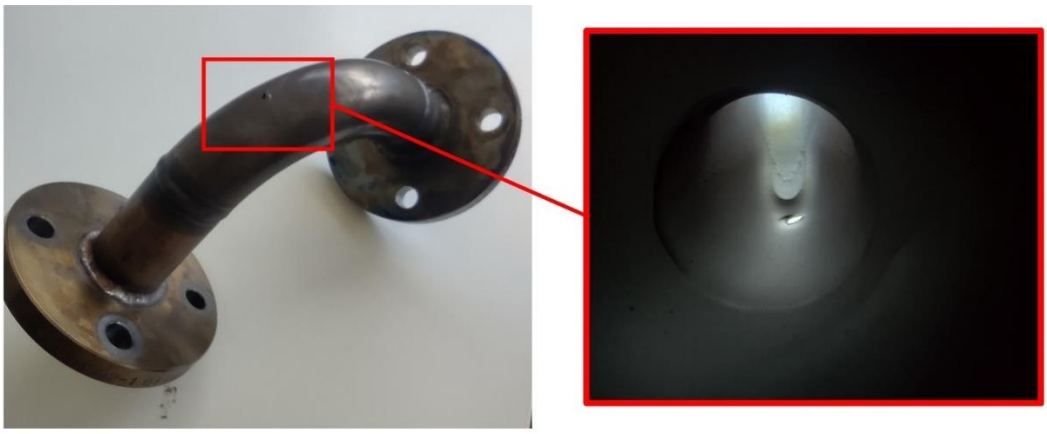

Figure 29: Erosion in the knee bend after 24h of operation.

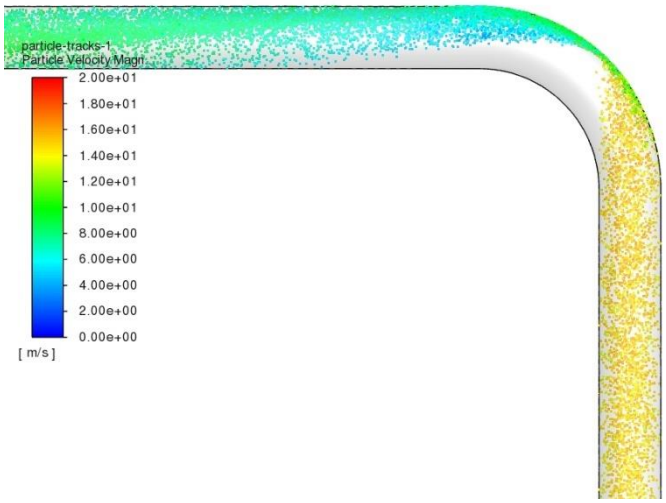

Figure 30: Analysis of the particle velocity prior the knee bend.

4 CONCLUSIONS

This report encompasses a design review of the particle heater loop, complemented by experimental results and associated remarks. The proposed particle heating technology underwent experimental testing, demonstrating that it enables safe operation and successfully fulfils the project goals. The experimental testing provided valuable information regarding operating conditions, energy requirements and lifetime assessment of critical components. This information will be further utilized in the design of the final test involving a sCO2/particles heat exchanger.